



Heart/liver-on-a-chip as a model for the evaluation of cardiotoxicity induced by chemotherapies

Pooneh Soltantabar^a, Erika L. Calubaquib^b, Ebrahim Mostafavi^{c,d,e}, Atefeh Ghazavi^a, Mihaela C. Stefan^{a,b,*}

^a Department of Bioengineering, University of Texas at Dallas, Richardson, TX, 75080, USA

^b Department of Chemistry and Biochemistry, University of Texas at Dallas, Richardson, TX, 75080, USA

^c Department of Chemical Engineering, Northeastern University, Boston, MA, 02115, USA

^d Stanford Cardiovascular Institute, Stanford University School of Medicine, Stanford, CA 94305, USA

^e Department of Medicine, Stanford University School of Medicine, Stanford, CA 94305, USA

ARTICLE INFO

Keywords:

Organ-on-a-Chip
Microfabrication
Drug metabolism
Cardiotoxicity
Doxorubicin

ABSTRACT

Drug discovery faces challenges due to the lack of proper preclinical tests, including conventional cell cultures and animal studies. Organ-on-a-chip devices can mimic the whole-body response to therapeutics by fluidically connecting microscale cell cultures and generating a realistic model of human organs of interest. Here, we describe a pumpless heart/liver-on-a-chip (HLC) using the HepG2 hepatocellular carcinoma cells and H9c2 rat cardiomyocytes to reproduce the cardiotoxicity induced by doxorubicin (DOX) *in vitro*. Cell studies confirmed the high viability of both cells up to 5 days of culture in HLC. The developed device demonstrated more significant damage to heart cells within the HLC than conventional static 3D culture in the case of DOX treatment, which is because of exposure of cells to both the parent drug and its cardiotoxic metabolite, Doxorubicinol (DOXOL). Our designed HLC device represents a unique approach to assess the off-target toxicity of drugs and their metabolites, which will eventually improve current preclinical studies.

1. Introduction

The pharmaceutical industry is in urgent need of enhanced drug discovery and development tools. It has been reported that it takes about 13.5 years and costs about \$2.5 billion for a drug to get into the market. Besides the exorbitant cost and time-consuming drug development process, 92 % of the drugs fail in human clinical trials (Von Aulock, 2019). There are ethical and scientific arguments arising from the usage of animals as the currently most common preclinical testing method. Animal studies impose suffering on the animals and stress for the researchers performing the experiments (Bottini and Hartung, 2009). Moreover, discoveries from animal studies do not effectively translate into the clinic due to differences between animal and human biology (Pistollato et al., 2016).

To address some of the limitations of preclinical tests, a new class of microfluidic devices was developed to replicate *in vivo* functions of organs on a microchip. This new technology, called “organ-on-a-chip” (Bhise et al., 2014; Polini et al., 2014), has been extended to “body-on-a-chip” (Misun et al., 2016; Guan et al., 2017; Lee and Sung, 2018) to

simulate multi-organ interactions. The organ-on-a-chip field is now progressing as a better tool for replicating human physiology by creating *in vivo*-like 3D tissue architectures *in vitro*. Within these devices, tissue explants, iPSC-derived cells, and cell lines as human organ representatives are connected fluidically in a closed system to answer various scientific questions (Von Aulock, 2019). Using these devices, scientists can mimic a physiologically relevant 3D microenvironment while providing the dynamic supplement of nutrients and multi-organ interaction (Lee and Sung, 2018).

When the number of organs increases, the complexity of the system increases, and consequently, several challenges in the design and interpretation of the results might appear; moreover, design complexity is related to determining appropriate organ sizes and media flow rate, which results in a physiologically realistic system that does not distort the nature of the interactions between organs. The interpretation complexity arises when researchers need to translate the experimental outcomes from these devices to *in vivo* responses in humans. Therefore, to understand the multi-organ interaction dynamics, robust mathematical tools can be implemented. These mathematical approaches are

* Corresponding author. 800 W Campbell Road, Richardson, TX, 75252, USA.
E-mail address: mihaela@utdallas.edu (M.C. Stefan).

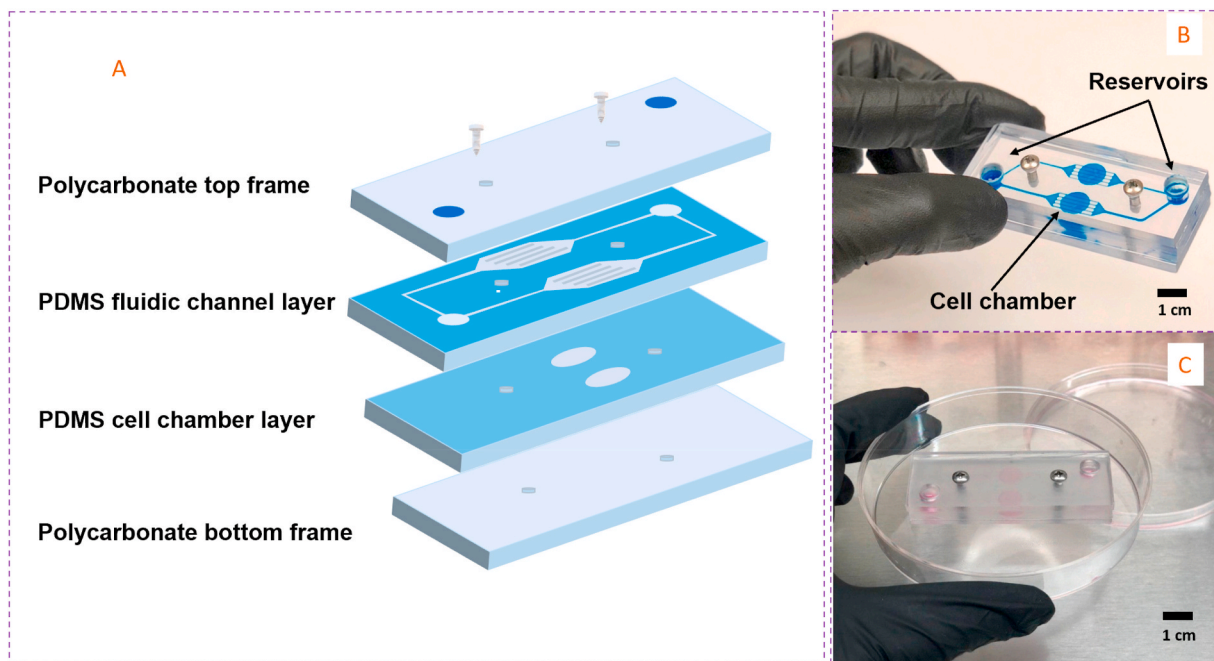


Fig. 1. Design and actual photograph of the two-layered pumpless microfluidic device. (A) Schematic illustration of the two-chamber cell culture layer and the device microfluidic channel layer (with the channels facing down), both made from PDMS. The cell chamber layer and the channel layer are sandwiched between two polycarbonate frames, and the system is secured with two stainless steel screws. (B) Photograph of the HLC with the CellTiter Blue dye flowing through the channels and chambers for better illustration of the microchannels and the reservoir. (C) Picture of the actual HLC assembled with a hydrogel containing the cells. The reservoirs are filled with the media, and the HLC is placed on a programmable rocker platform to create gravity-induced flow. (For interpretation of the references to color in this figure legend, the reader is referred to the Web version of this article.)

developed from mathematical methods that have been used in biological and pharmacological sciences for a long time (Sung et al., 2019).

Shuler et al. (Ghanem and Shuler, 2000; Sung and Shuler, 2000; Sung et al., 2010) designed a series of pioneering devices guided by the concept of a mathematical model known as a physiologically based pharmacokinetic-pharmacodynamic (PBPK-PD) model aimed at reproducing the multi-organ interactions within the body for drug toxicity testing. The term pharmacokinetics (PK) is used for the time-dependent concentration of a substance in a living system (Gerlowski and Jain, 1983). A PBPK model is built on physiological considerations where the human body is segregated into compartments with various cell lines representing different organs that are fluidically connected. Pharmacodynamics (PD) seeks to characterize the time course of drug effects through the application of mathematical modeling (Mager et al., 2003). Integration of the PK of a drug with the subsequent *in vivo* pharmacological response (PK/PD modeling) has been extended to all phases of drug development (Peck et al., 1992).

The Shuler group first examined the possibility of coupling the PK/PD modeling with a microfluidic device (Sung et al., 2010). They applied residence-time scaling where the residence times of medium in each organ compartment were matched to blood residence times in the *in vivo* counterparts, letting the organs within the device be exposed to drugs for the same length of time as the human organs are exposed *in vivo*. Most of their early designs required external pumps, however pumpless devices which work based on gravity-induced flows, are economical, operate with physiologically realistic shear stress (less than 2 dyn cm^{-2}) on cells, and can prevent bubble formation or entrapment, which is a significant problem in microfluidic devices (Kim et al., 2007).

One of their studies compared the PK profile of the doxorubicin (DOX) anticancer drug predicted from a multi-organ-on-a-chip to the data expected in the human body. This study illustrated an early integration of microfluidic devices and PK modeling (Tatosian and Shuler, 2009). They showed that a specific combination of drugs could inhibit the proliferation of a multidrug-resistant variant of uterine cancer. They

were able to scale up the result to calculate doses *in vivo*. In another study, the same group managed to link a three-organ micro-engineered cell culture device with computational PK/PD models. A proof-of-concept study showed that a PBPK-PD could be used as a mathematical platform to model the toxicity of 5-fluorouracil (5FU) anticancer drug on hepatocyte, colon carcinoma, and myeloblast cell lines. In this analysis, an experimental cell death study was applied to numerically fit the computational model's parameters for generating the best estimates of cell death *in vivo*.

One of the main challenges in drug discovery for cancer therapy is the cardiotoxicity associated with anticancer drugs (Albini et al., 2010). Moreover, in our previous study (Soltantabar et al., 2020), we demonstrated that the cardiotoxicity induced by anticancer drug DOX could be alleviated by co-administration of DOX with natural antioxidants. DOX is an anthracycline anticancer drug that interferes with the synthesis of DNA and RNA by inhibiting the separation of DNA double helix, an essential step for cell proliferation (Tacar et al., 2013). Although DOX can effectively combat the rapid division of the cells and is known as one of the most potent chemotherapeutic drugs approved by the Food and Drug Administration (FDA) (Carvalho et al., 2009), it causes toxicity to the major organs, especially life-threatening cardiotoxicity (Tacar et al., 2013). While the mechanism of this cardiotoxicity induced by DOX is not fully understood yet, some studies are showing that one of the means of this cardiotoxicity can be attributed to doxorubicinol (DOXOL), the primary metabolite of DOX (Hanna et al., 2014; Kamei et al., 2017). Previous studies showed that DOXOL is significantly more potent than DOX at compromising systolic and diastolic cardiac function. An exciting feature of the organ-on-a-chip technology is capturing this off-target cardiotoxicity by developing systems incorporating liver and heart components on a single chip. Oleaga et al. (2018) investigated the effect of hepatic metabolism on off-target cardiotoxicity in a system with cardiac and liver components. They built a device by combining multielectrode arrays for electrical measurements and silicon cantilevers for mechanical measurements. Using this multi-organ microfluidic

platform, they demonstrated that the liver reduced the cardiotoxicity of a cardiotoxic parent by metabolizing it to nontoxic metabolites and increasing the cardiotoxicity of a nontoxic parent liver was metabolized to toxic metabolites. In another study, Michael Shuler's group developed a four-organ chip for toxicity testing comprising liver, heart, skeletal muscle, and neurons using readouts for cardiac, skeletal muscle contraction force, and neuron electrophysiological data. These cell types were chosen to provide insight into significant metabolic and functional changes in human tissues in response to model drugs whose toxicity was well-defined. The results of all drug treatments over a 14-day culture period in constant media circulation within the device were in general agreement with published toxicity results from human and animal data (Oleaga et al., 2016).

Here we introduced a pumpless device named Heart/Liver-on-a-chip (HLC) that enables the culture of two different cell lines in a closed loop of gravity-induced flow. The cell lines used in this study were HepG2 hepatocellular carcinoma cells and H9c2 rat cardiomyocytes. As the representative of cardiomyocytes, we used this permanent cardiac cell line characterized by several cardiomyocytelike properties (Hescheler et al., 2017). H9c2 cells, which are most often used as a cardiac cell model for routine cytotoxicity screening (Oleaga et al., 2016; Hescheler et al., 2017; Xue et al., 2018), have been extensively used in organ-on-a-chip devices as well (Chegaev et al., 2013; Choi et al., 2007; Giridharan et al., 2010). Therefore, we decided to use them in our research for simplicity and proof of concept. As the HLC performs without any pumps, the width of the channels across the chambers was calculated to achieve the desired flow rates. The fluid dynamics of the system was characterized to confirm that the residence time of the media in each chamber matches the residence time of the blood in the associated organ within the body. We then thoroughly investigated the viability of the cells cultured in HLC compared to conventional cell culture platforms, including static 2D and 3D cultures. Drug testing was finally performed within the HLC to investigate whether this device can produce the metabolite of interest and to indicate whether HLC can serve as a proof of concept tool for recreating the cardiotoxicity induced by anticancer and its metabolite *in vitro*. The integration of metabolizing components to *in vitro* models, which cannot be studied through conventional preclinical platforms, would improve the prediction of drug toxicity studies. These models have the potential to more realistically capture both the efficacy and the side effects of newly developed drugs, leading to tremendous time and cost savings.

2. Materials and methods

2.1. Overall device description and design

Our design was inspired by two pumpless layered designs reported by Shuler (Sung et al., 2010; Hsiao et al., 2015). However, our design was based on a 3D cell culture environment while carrying out a 2D monolayer design. Additionally, here we employed different types of cells (heart and liver cells) to investigate the cardiotoxicity of anticancer drug. At the same time, in their design, they incorporated tumor and liver cells to investigate the anticancer activity. The HLC contains two polydimethylsiloxane (PDMS) layers, which separate the fluidic channel layer and cell culture chamber layer inserted between two polycarbonate frames (Fig. 1A). The whole device was secured and held together using two stainless steel screws. The culture chambers accommodate both liver cancer cells and heart cells in separate chambers, which are fluidically linked through the channel layer that is placed on top of them, so the circulating media is shared between two cell types.

Because there is no external pump in the system, the width of the channels was the controlling factor for the fluid dynamic of the system, which was designed to mimic the residence time of the blood in each associated organ in the body. All HLC parts were selected from an autoclavable and transparent material to facilitate the operation and

Table 1

Physiological information and the performed calculation to estimate the flow-rate of channels within the HLC.

Organ	Volume in the body (mL) (Price et al., 2003)	Flow rate in the body (mL/min) (Price et al., 2003)	Residence time (s)	Volume in the device (μL)	Flow rate main channels in the device (μL/s)
Heart	360	730	29.6	25.13	0.85
Liver	1350	1566	51.72	25.13	0.48

usage. A photograph of the actual assembled HLC injected with dye for better visualization is shown in Fig. 1B.

2.2. Channel layer design

Designing an organ-on-a-chip that is physiologically realistic is essential as the flow between the chambers can influence the PK of the device (Lee et al., 2017). To achieve this goal, we designed our HLC by scaling based on residence time (Hsiao et al., 2015; Kobuszewska et al., 2017). In this method, the cells will be exposed to drugs with the same duration that the cells in native organs in the body are exposed (Hsiao et al., 2015; Kobuszewska et al., 2017). First, the residence time of the blood in each organ in the body was calculated by dividing the organ size by the flow rate of the blood in each organ (Price et al., 2003). Based on the residence time scaling, the residence time of the blood in each organ of the body should be the same as the residence time of the media in an associated organ within HLC; thus, the flow rate of the media to each chamber can be calculated. By substituting the flow rate of each chamber in Hagen–Poiseuille's equation (equation (1)) for gravity-induced flow (and substituting Δh by $L \times \text{Sine}(\alpha)$; α = tilting angle), the hydraulic radius, the cross-section area of each channel and finally the width of each channel can be calculated (Sin et al., 2004; Price et al., 2003).

$$Q = \frac{\rho g \pi \Delta h R_H^4}{8 \mu L} \quad (1)$$

where Q is the flow rate generated by the pressure difference, ρ is the density of the media (1009 g/m³), g is the gravity constant (9.8 m/s²), Δh is the height difference (m), R_H is the hydraulic radius of the channel (m), μ is the fluid viscosity (0.001011 Pa s), and L is the channel length (m). By using this approach, the channel dimension for each chamber was calculated to achieve the desired flow rate. The residence time and expected volumetric flow rate for each organ were calculated and presented in Table 1.

2.3. Microfabrication of HLC

To develop the channel layer, PDMS prepolymer (Sylgard 184, Dow Corning) was mixed with a hardener with a ratio of 10:1 and was dispensed on a 4-inch silicon wafer master followed by curing at 70 °C for 30 min. The master for the channel layer was made by soft lithography. SU-8 2100 photo epoxy (Kayaku Advanced Materials, Inc., MA, USA) was selected as it is suitable for creating relatively thick features (250 μm in this case) on the silicon wafer. The photoresist was spin-coated on the silicon wafer with different spin speeds to obtain the desired thickness. The 250 μm thickness was obtained by spinning at 500 rpm spin speed with an acceleration of 100 rpm/s for 20 s followed by a 1380 rpm spin speed with 300 rpm/s acceleration for 30 s. Spin coating was followed by soft baking performed at 65 °C for 7 min and 95 °C for 60 min based on SU8 2100 datasheet. The spin-coated SU8 layer was patterned by UV exposure at an exposure dose of 360 mJ/cm² using the designed photomask. The photomask pattern was created using Autodesk software, and the mask was fabricated at The University of Texas at Dallas cleanroom facility. The post-exposure bake was

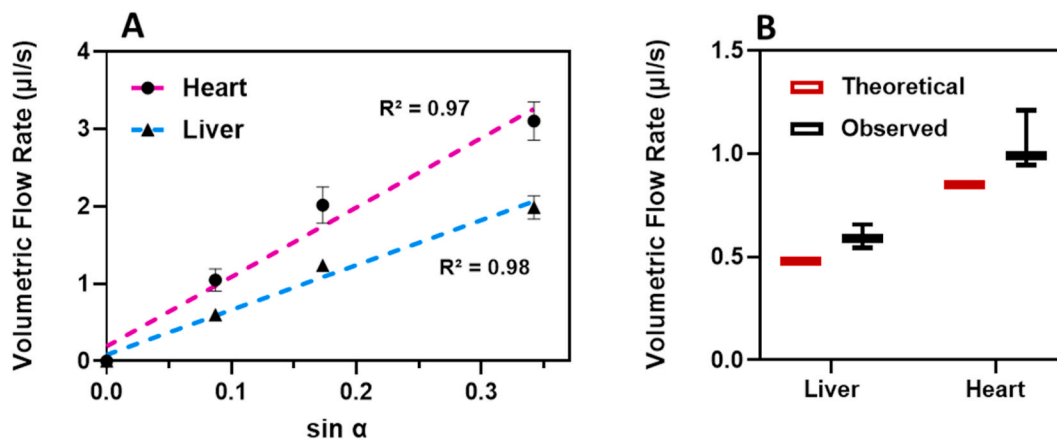


Fig. 2. The fluid dynamic of the device. (A) The device was set on the 3 different angles (5, 10, and 20°). The flowrate associated with each chamber was measured and plotted versus the tilting angle. A linear relationship between the volumetric flow rate and the height (tilting angle) was observed, which is in agreement with the Hagen–Poiseuille’s equation (1). (B) Volumetric flow rate of the media for each chamber shows that the calculated flow rate is comparable with the observed flow rate in device. Slightly higher flow rate within the device compared to the theoretical one is due to the high sensitivity of the flow rate to imperfections of microfabricated channels.

performed at 65 °C for 5 min and 95 °C for 40 min. To develop the SU8 structure, the master was then immersed in the SU8 developer (Kayaku Advanced Materials, Inc., MA, USA) for 30 min. The frame of the device was milled out of a 5 mm thick polycarbonate sheet at a machine shop located at the University of Texas at Dallas. The cell culture chamber layer was made from a commercially available PDMS sheet with a thickness of 0.5 mm. The two cell chambers were created using a biopsy punch with a diameter of 8 mm, which were later filled with hydrogel-encapsulated cells.

2.4. Device degassing and assembly

The surface of the PDMS is hydrophobic, which limits its usage in applications involving aqueous solutions. Bubbles tend to stick to the surface of the PDMS, which results in their entrapment during the device assembly, causing problems for the cells by flow blockage. With some modifications to a previously developed method by Wang, we could prevent bubble formation in the HLC by combining surface treatment and a vacuum filling method (Wang et al., 2012).

The PDMS layers were oxygen plasma-treated at 50 W for 120 s to make the parts hydrophilic. All HLC parts were immersed in 70 % EtOH. The container, including device parts soaked in EtOH, was then transferred to a desiccator connected to a vacuum for 30 min. The device parts were rinsed with PBS solution and were transferred to another container filled with PBS +5 % fetal bovine serum (FBS), then the device parts were vacuumed for another 60 min. After vacuuming, the device parts were autoclaved for 30 min at 125 °C while still immersed in PBS and FBS solution. The device assembly was done from bottom to top. The cell chamber layer was placed on top of the bottom polycarbonate frame. The chambers were filled with PGmatrix encapsulated cells, followed by PGwork addition and incubation for 1 h inside an incubator for effective crosslinking. The cell chamber layer was removed from the incubator and flooded with media to minimize air contact during assembly. Finally, the channel layer was placed on the top (with the channels facing down). The system was fixed and secured using the screws, and the reservoirs were filled with media. The device was placed in a sterile 100 mm petri dish and was placed on a tilting rocker inside an incubator.

2.5. Cell culture

HepG2 hepatocellular carcinoma cells and H9c2 rat cardiomyocytes were purchased from American Type Culture Collection. The cells were

maintained in Dulbecco’s modified Eagle medium supplemented with 10 % (v/v) FBS and 1 % (v/v) penicillin/streptomycin in an incubator at 37 °C and 5 % CO₂. Cell culture media was changed every three days.

For further characterization of the HLC, the rocker was set on three different angles (5, 10, and 20°), and the flow rate at each angle was measured in channels. Based on the Hagen–Poiseuille’s equation (1), which was the basis of our design, the flow rate is supposed to be linearly proportional to Δh , which is the height difference, and consequently linearly proportional to Sine (α) as Δh is equal to $L \times \text{Sine}(\alpha)$ (where α = tilting angle). The experimental data from this study is presented in Fig. 2A. The high R^2 value of the plot indicates that the claim is valid, and the observed flow rates are close to the theoretically calculated flow rate from Hagen–Poiseuille’s equation (1).

To make 3D construct of cells, a suspension of cells in PGmatrix with a concentration of 10^7 cells/mL was prepared based on the manufacturer’s guide. The cells were detached from the confluent flasks of cells using trypsin/ethylenediaminetetraacetic acid (EDTA). After adding media for neutralization of trypsin/EDTA, the cell pellet was obtained by centrifugation at $125 \times g$ for 5 min. Cells were resuspended in media, followed by adding PGwork. After homogenizing the cell suspension, PGmatrix was added. Based on the manufacturer’s protocol, the added PGwork was 4 % of pure PGmatrix solution. 20 μL of each cell suspension were added to 96 well plate and device cell chambers for cell culture in static 3D and device, respectively. After 1 h of incubation at 37 °C and 5 % CO₂, 100 μL of DMEM was added to each well for static study. In the case of the device, the cell chamber layer was flooded with media, the channel layer was placed on top, and the system was closed using the screws.

2.6. Characterization of fluid dynamics in the system (flowrate and distribution)

To investigate the fluid dynamics, the device was assembled as described above. However, the cells were not encapsulated into the hydrogel for this study, and the reservoirs were filled with media. The flow rate of the media in each channel was measured by a video capturing method developed by Shuler et al. (Miller and Shuler, 2016). The assembled device was placed on the rocker at different angles (5, 10, and 20°). A dye was injected into the reservoir at a higher position, and the video was recorded while the dye was flowing into the channels. By measuring the time that dye traveled at a specific length in the channel, the linear flow rate was calculated and afterward multiplied by the cross-section area of each channel to calculate the volumetric flow rate.

The experiment was performed in triplicate, and the average linear flow rate was calculated. A video of dye injection into the HLC is included in the Supplementary Information.

The flow distribution study was performed to investigate whether the reservoirs will reach an equilibrium concentration after the injection of an agent to the system with the selected rocker tilting pattern. For this study, the device was placed on the rocker with one reservoir at a higher position on the rocker with a tilting angle of 5°, which was the base of our calculations. At $t = 0$, 10 μL of media was removed and replaced with the same volume of the CellTiter Blue dye, and then the device started to tilt on the rocker. Two different tilting programs were tested on the device: (1) 30 splits, where one side is up for 30 s, then the other side is up for 30 s, and (2) 60 splits, where one side is up for 60 s, then the other side is up for 60 s. At specific time intervals, 5 μL of media sample was removed from each reservoir and was collected in a microcentrifuge tube. This study was performed by setting multiple devices on the rocker. The samples were then subjected to UV-Vis spectroscopy to record the absorbance of samples at the wavelength of 600 nm to quantify the amount of dye in each sample. Due to the small sample size, regular UV-Vis spectroscopy was not possible, so a Nanodrop instrument was used to collect the absorbance data.

2.7. Cell viability in the device (2D vs. 3D & 3D vs. device)

Viabilities of both heart cells and liver cancer cells were studied and compared in 3 different platforms: conventional 2D culture, static 3D culture, and the device. For 2D culture, the cells were trypsinized and cultured in 96 well plates with a density of 10^4 cells per well. For static 3D and device, cells were incorporated into the hydrogel with the cell density of 4×10^6 cells/mL in the PGmatrix (crosslinking process described above). 20 μL of samples were added to 96 well plates for static 3D and to cell chambers within the device. The volume of cell chambers in the device was 25 μL , about 20 % of this total volume of the chamber was left empty to provide some space for media flow over the cells.

On days 1, 3, and 5 after culture, the viability of the cells was assessed using a commercial live/dead assay kit (Molecular Probes). For this assay, the ethidium homodimer-1 red dye (2 $\mu\text{L}/\text{mL}$ in PBS) for dead cells and calcein-AM green dye (0.2 $\mu\text{L}/\text{mL}$ in PBS) for live cells were mixed. For 2D and static 3D, 96 well plates were used for imaging, however in the case of culture in the device, the device was disassembled, and the hydrogels were transferred to a 35 mm petri dish for subsequent staining and imaging. After incubating the cells with dyes for 15 min, the cells were washed a few times with PBS, and the images were obtained using the Cytation 3 fluorescent microscope.

2.8. Cell functional evaluation through urea synthesis

To quantify the level of urea production by cell lines, in both static monocultures and device, a DIUR assay kit (BioAssay Systems, Hayward, CA) was used. For static monocultures, HepG2 and H9c2 cells were cultured separately in 96 well plates with a cell density of 4×10^6 cells/mL, and 150 μL of media was added to each well. For culture in the device, three different conditions were studied: HepG2 only, H9c2 only, and HepG2+H9c2 co-culture in the device (as described above). In the case of monocultures in the device, the other chamber was filled with hydrogel only (with no cells incorporated). At days 1, 3, and 5, with day 1 corresponding to 24 h after the culture in 96 well plates and device assembly, 50 μL culture media was collected in 96 well plates and were stored at -80°C for later measurements. 100 μL of the chromogenic reagent was added to each well resulting in a stable colored complex with urea, which was incubated at room temperature for 20 min. Finally, the optical density was measured at 430 nm using a BioTek Cytation 3 fluorescent microscope. The concentrations were calculated and reported in mg/dl by comparing to a standard curve.

2.9. Investigation of in Vitro DOX metabolism by HepG2 cells

To investigate the ability of HepG2 cells to metabolize the DOX within *in vitro* 3D culture, the cells were cultured in 3D hydrogels in 96 well plates as it was described above. 24 h after the culture, media was replaced by DMEM containing 1 μM (543.2 ng/mL) DOX. At specific time points (up to 72 h) the media was collected and was stored at -20°C for further quantification of DOX and its cardiotoxic metabolite DOXOL.

2.10. Analytical liquid chromatography-mass spectrometry (LC-MS) condition

Compound levels for cellular stability were monitored by LC-MS/MS using an AB Sciex (Framingham, MA) 4000 QTRAP® mass spectrometer coupled to a Shimadzu (Columbia, MD) Prominence LC. Analytes were detected with the mass spectrometer in positive MRM (multiple reaction monitoring) modes by following the precursor to fragment ion transitions indicated here: **DOX**: 544.171 to 397.000; **DOXOL**: 546.198 to 399.100. An Agilent C18 XDB column (5 μm , 50 \times 4.6 mm) was used for chromatography with the following conditions: Buffer A: $\text{dH}_2\text{O} + 0.1\%$ formic acid, Buffer B: acetonitrile + 0.1 % formic acid, 0–2 min 5 % B, 2–3.5 min gradient to 60 % B, 3.5–5 min 60 % B, 5–5.1 min gradient to 5 % B, 5.1–7.5 5 % B. Daunorubicin (transition 528.147 to 321.000) was used as an internal standard (IS). All measurements were performed in triplicate, and average responses with associated error bars are presented in Fig. 2B.

2.11. Sample preparation for LC-MS/MS analysis

At varying times (0 h, 3 h, 6 h, 12 h, 24 h, 48 h, and 72 h) post addition of 1 μM doxorubicin to the HepG2 cultures, media was removed, and the lysate precleared of protein by the addition of a two-fold volume of acetonitrile containing 100 ng/mL of internal standard (daunorubicin) followed by vortexing and incubation at room temperature or 10 min. After two steps of centrifugation at $16,000 \times g$ for 5 min. The supernatant was analyzed by LC-MS/MS for levels of doxorubicin and doxorubicinol. Compound levels were quantitated in reference to standard curves prepared by adding varying concentrations of doxorubicin and doxorubicinol to untreated blank cell media and processing, as described above. The concentrations of drug in each time-point sample were quantified using Analyst software (Sciex). A value of 3-fold above the signal obtained from blank plasma or tissue homogenate was designated the limit of detection (LOD). The limit of quantitation (LOQ) was defined as the lowest concentration at which back-calculation yielded a concentration within 20 % of theoretical.

2.12. Cell treatment in the device

For cell treatment, the device and static controls were set as described above. DOX was dissolved in DMSO to give a 10 $\mu\text{g}/\mu\text{L}$ stock solution. The stock solution was then added to DMEM media to make the desired concentrations. The final DMSO concentration in media was set to be less than 0.1 % (v/v) to avoid any toxic effect of the solvent. For controls, the cells were treated with a comparable amount of DMSO (without drug). 24 h after cell culture in the device and in 96 well plates (for static controls), media was changed with media containing the drug. During the cell treatment, the device was placed in a petri dish to minimize the media evaporation. All assembled devices and static controls were placed in a humidified incubator at 37°C under 5 % CO_2 .

2.13. Flow cytometry analysis

After 24 h drug treatment, the hydrogels were harvested from the device chambers (after the disassembly) or static 3D cultures and were collected in a microtube. For flow cytometry analysis, the cells were

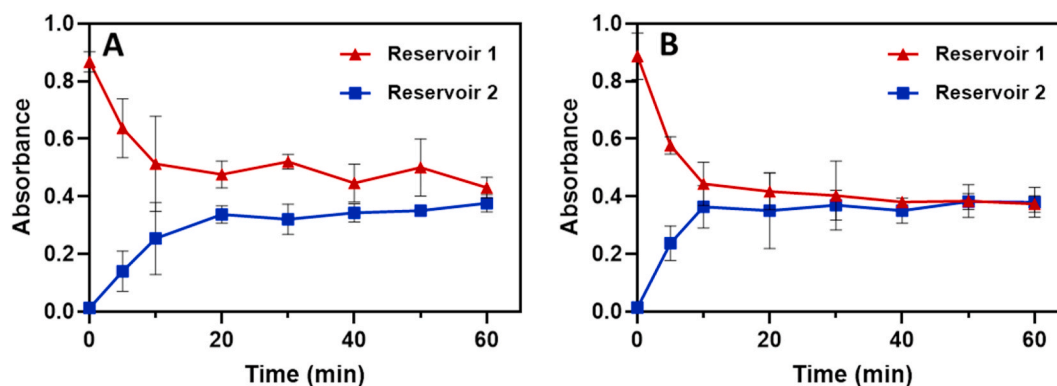


Fig. 3. Dye distribution in the microfluidic device. The dye distribution within the device was investigated by injecting Cell TiterBlue dye into one of the reservoirs and setting the device in motion on a rocker, then taking samples of each reservoir at specific time points. The samples were then subjected to spectroscopy at a wavelength of 600 nm to quantify the amount of dye in each sample. (A) Overall dye distribution in device with 30 s splits. (B) Overall dye distribution in device with 60 s splits.

needed to be recovered from the gel. For the cell recovery, the gel was mechanically disrupted thoroughly by pipetting. 100 μ L PBS was added to the tube, and the mixture was pipetted thoroughly, followed by centrifugation at $400\times g$ for 5 min. The supernatant was then removed, and the cell pellet was used for the staining to discriminate the early stage of apoptosis from necrosis. Alexa Fluor 488 annexin V/Dead Cell Apoptosis Kit (catalog no. V13241) were purchased from Invitrogen Life Technologies (Carlsbad, CA) and was used according to the manufacturer's instructions. This kit provides a rapid and convenient assay for apoptosis. Briefly, the cells were re-suspended in 100 μ L of the kit's specific binding buffer. 5 μ L Alexa Fluor 488 annexin V and 1 μ L of 100 μ L/mL PI working solution (in binding buffer) was added to the cell suspension. After 15 min of incubation at room temperature, the final

volumes were adjusted to 500 μ L, and the samples were transferred on ice for flow cytometry analysis measuring the fluorescence emission at 530 nm and 575 nm and the excitation of 488 nm (using the FITC and PE filters).

2.14. Statistical analysis

All data analyses were performed using GraphPad Prism Software version 8. A significant difference between 2 groups was evaluated using the F-test to compare variances followed by the student t-test. In contrast, for meaningful difference evaluation between 3 or more groups, one-way and two-way ANOVA was performed. A P-value of <0.05 was considered to be significantly different.

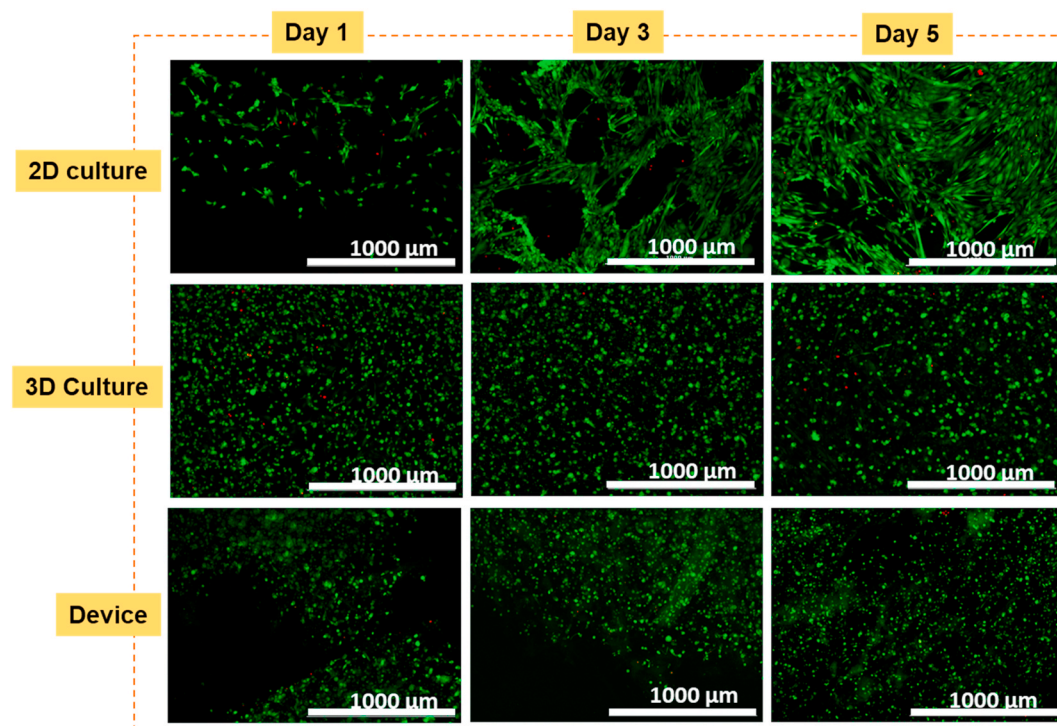


Fig. 4. Fluorescent micrographs of H9c2 cells cultured in conventional 2D, 3D, and device. Live/dead assay was performed to assess the cell viability of H9c2 cells in 3 different platforms: static 2D culture (top), static 3D culture by embedding the cells in hydrogel (middle), and 3D culture within the device (bottom). For 3D culture, the cells were incorporated into the hydrogel and were pipetted into the 96 well plates. For device culture, the same hydrogel as static 3D was used. The cells were embedded in the hydrogel and were introduced to the device chambers. After 1 h, when the gelation was complete, the device was assembled, and the reservoirs were filled with media. On days 1, 3, and 5 post-culture, the cells were stained with live/dead assay kit to visualize the live cells (green) and dead cells (red) for further imaging. (For interpretation of the references to color in this figure legend, the reader is referred to the Web version of this article.)

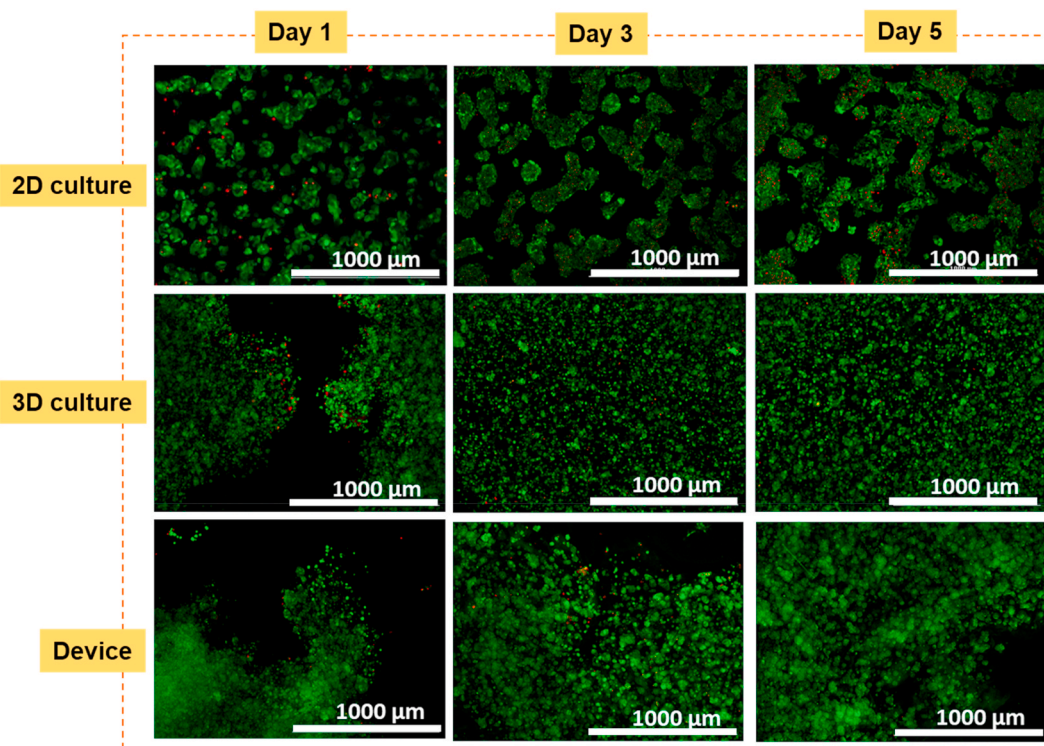


Fig. 5. Fluorescent micrographs of HepG2 cells cultured in conventional 2D, 3D, and device. Live/dead assay was performed to assess the cell viability of HepG2 cells in static 2D culture (top), static 3D culture (middle), and 3D culture within the device (bottom). For 3D culture, the cells were incorporated into the hydrogel and were pipetted into the 96 well plates. For device culture, the gels containing the cells were introduced to the device chambers. After 1 h, when the gelation was complete, the device was assembled, and the reservoirs were filled with media. On days 1, 3, and 5 post culture, the cells were stained with live/dead assay kit to visualize the live cells (green) and dead cells (red) for further imaging. (For interpretation of the references to color in this figure legend, the reader is referred to the Web version of this article.)

3. Results and discussion

3.1. Fluid dynamic of the device

The linear flow rate of media in each channel was measured by video recording after dye injection to one reservoir. Fig. 2B shows the calculated volumetric flow rate versus the observed flow rate. The calculated flow rate for the heart and liver chambers were 0.85 and 0.48 $\mu\text{L/s}$, respectively. The experiment was performed in triplicate, and the average observed flow rate for heart and liver chambers was 1.04 ± 0.14 and 0.59 ± 0.05 $\mu\text{L/s}$, respectively. In general, the predicted and observed flow rate were comparable. The results indicated that the observed flow rate was slightly higher than the calculated flow rate for both chambers. Similar discrepancies were observed by Shuler et al., (Miller and Shuler, 2016) which was attributed to the high sensitivity of flow rate to small changes and imperfections in the device. As was

demonstrated in equation (1), the hydraulic radius is correlated to the flow rate by the power of four; therefore, small changes in the radius results in significant deviations from the predicted flow rate.

The flow distribution studies were performed by injecting CellTiter Blue dye into one of the reservoirs, starting the rocker to tilt at two different programs, and taking samples from both reservoirs at specific time points. The samples were collected in microtubes, and the absorbance was measured at 600 nm using a nanodrop device as the volume of the collected sample was very low. The results revealed that by setting the rocker at 30 s splits program (one side up for 30 s, then the other side up for 30 s), the reservoirs did not reach an expected equilibrium concentration after 1 h of rocking on the device. However, after injecting the dye to one of the reservoirs and applying the 60 s splits program (one side up for 60 s, then the other side up for 60 s), both reservoirs could reach an equilibrium concentration only after about 40 min of tilting on the rocker, which is an indicator of better dye distribution at this rocking

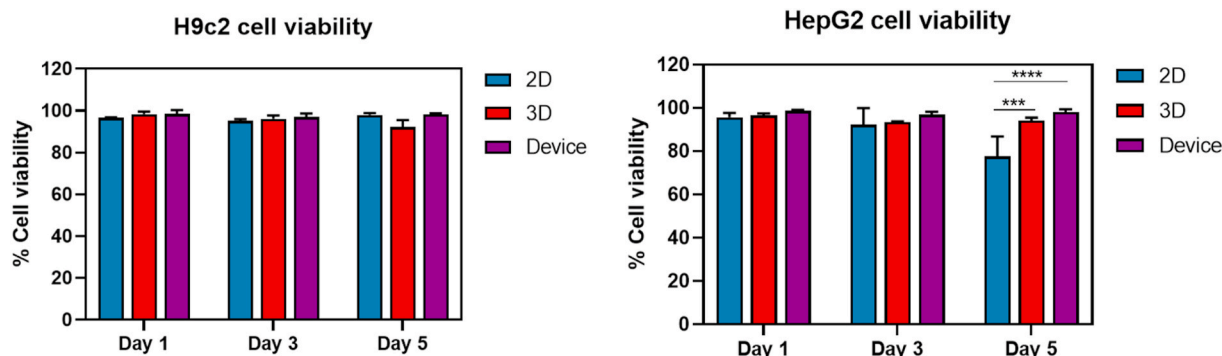


Fig. 6. Viability of the H9c2 and HepG2 cells in device versus static 2D and 3D controls.

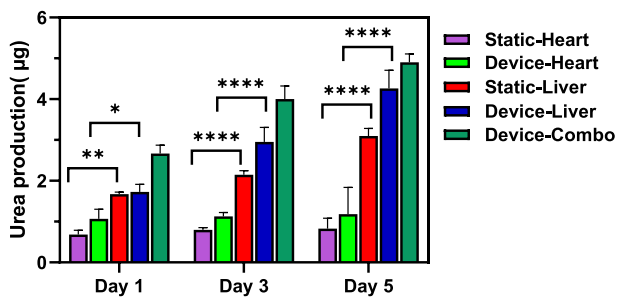


Fig. 7. Characterization of the functionality of the cells through urea synthesis. Urea production of the rocked device versus the static 3D culture was quantified using a DIUR assay kit by taking samples of the culture media on days 1, 3, and 5 post culture. For the conventional static cultures, cells were embedded into the hydrogel and were added to the 96 well plates. For culture in the device, 3 different conditions were tested: H9c2 cells alone, HepG2 cells alone (where the other chamber within the device was filled with hydrogel only without any cells), and both cells cultured in the device in their specific chambers. The urea production was increased significantly in a dynamic environment of the device compared to static culture. Error bars indicate the standard error of the means, asterisks mark significance levels of $p < 0.05$ (*), $p < 0.01$ (**), $p < 0.0001$ (****), and $n = 3$.

program. Fig. 3 shows the absorbance data versus time for both 30 s splits and 60 s splits programs.

3.2. Cell viability

Figs. 4 and 5 represent the live/dead staining of H9c2 and HepG2 cells that were cultured in 2D, 3D, and device to investigate whether the device can keep the cells healthy and viable for five days post culture. The quantitative cell viability values are presented in Fig. 6. As shown, there was no significant difference in the viability of H9c2 cells in 2D, 3D, and device cultures over a 5-day culture, where all three platforms showed the viability of more than 90%. A similar trend was observed for HepG2 cells on days 1 and 3; however, on day five, the viability in 2D culture was about 17% and 21% lower than 3D and device, respectively. This can be due to the clumping of HepG2 cells, which prevents the cells from receiving enough nutrients in 2D culture after five days. Additionally, the viability of HepG2 cells significantly increased in

device compared to 2D and static 3D, which can be attributed to media circulation and better penetration of nutrients into the hydrogel. In general, this experiment demonstrated that the device could support high cell viability for both H9c2 and HepG2 cells over a 5-day culture.

Values are shown as the average percentage viable ($n = 3$). H9c2 cells (left) demonstrated similar and very high (above 90%) cell viability in all three platforms throughout a 5-day culture. However, the HepG2 cells (right) demonstrated similar and very high (above 90%) cell viability in all three platforms only up to day 3 of the culture. On day 5 post culture, the viability of 2D culture dropped below 80%, which might be due to the tendency of these cells to grow in clumps, and some cells in lower layers were not exposed to enough nutrients from the culture media. Error bars indicate the standard error of the means, asterisks mark significance levels of $p < 0.001$ (**), $p < 0.0001$ (****), and $n = 3$.

3.3. Urea quantification

The inability to produce urea in hepatocytes can be an indicator of the hepatic damage (Bolley et al., 2015). Urea production by heart and liver cells were assessed throughout the culture period by analyzing the media removed from the device and the static culture on days 1, 3, and 5 post-culture (Fig. 7). The devices ($n = 3$) were assembled as described above, and the urea production was compared to static 3D culture for the monocultured and co-cultured cell lines. The results indicated that in the case of HepG2 cells, the hepatic function was improved in a 3D dynamic environment within the device. For instance, on day five post-culture, the urea production was $3 \pm 0.18 \mu\text{g}$ in static culture while the urea was quantified as $4.3 \pm 0.44 \mu\text{g}$ for the device on the same day. This observation could be due to significant induction of CYP1A1 and CYP3A4 enzymes, which have pivotal roles for drug metabolism, in dynamic culture within the device compared to static culture as reported by the Shuler group (Miller and Shuler, 2016). However, a similar trend was not observed for heart cells, and there was not any significant difference between the urea production of heart cells in the device and static 3D culture. Moreover, the results of this experiment show that the co-culture of cells in the device does not seem to have any significant impact on the total urea production compared to monocultures, which was similarly observed by Oleaga et al. (2018) Altogether, these results demonstrate the improvement in overall liver function within the device

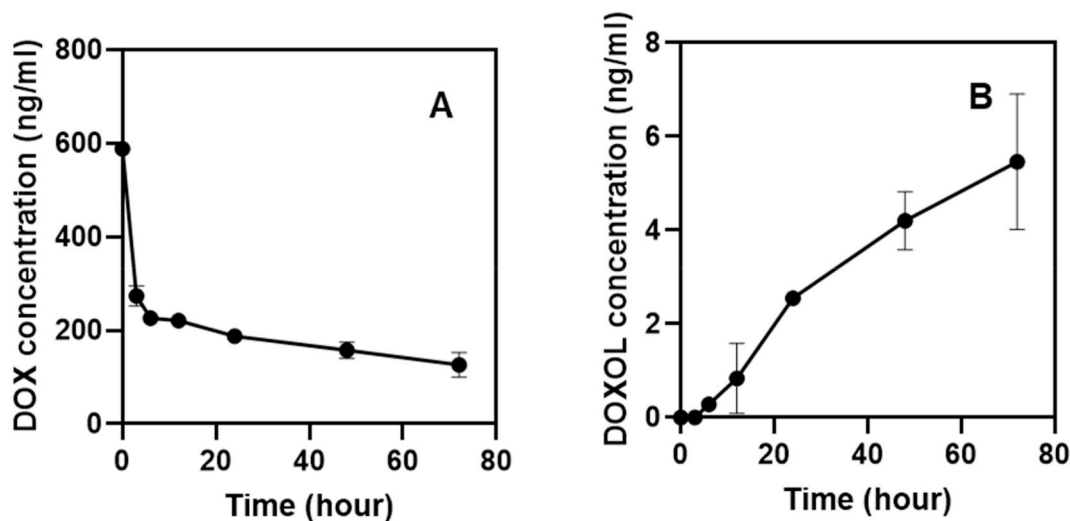


Fig. 8. Measured DOX and DOXOL in the culture medium during the incubation of the HepG2 cells in 3D culture. The media was collected at specific time points, and after the protein precipitation, the samples were analyzed using LC-MS. (A) The amount of the DOX measured in the media indicated that more than 70% of initial DOX added to the culture medium was metabolized by HepG2 cells after 72 h of incubation. (B) The amount of DOXOL produced by the HepG2 cells in the media. The detection of DOXOL in the media indicates that the liver cells can effectively metabolize DOX and produce the cardiotoxic metabolite DOXOL *in vitro* setting.

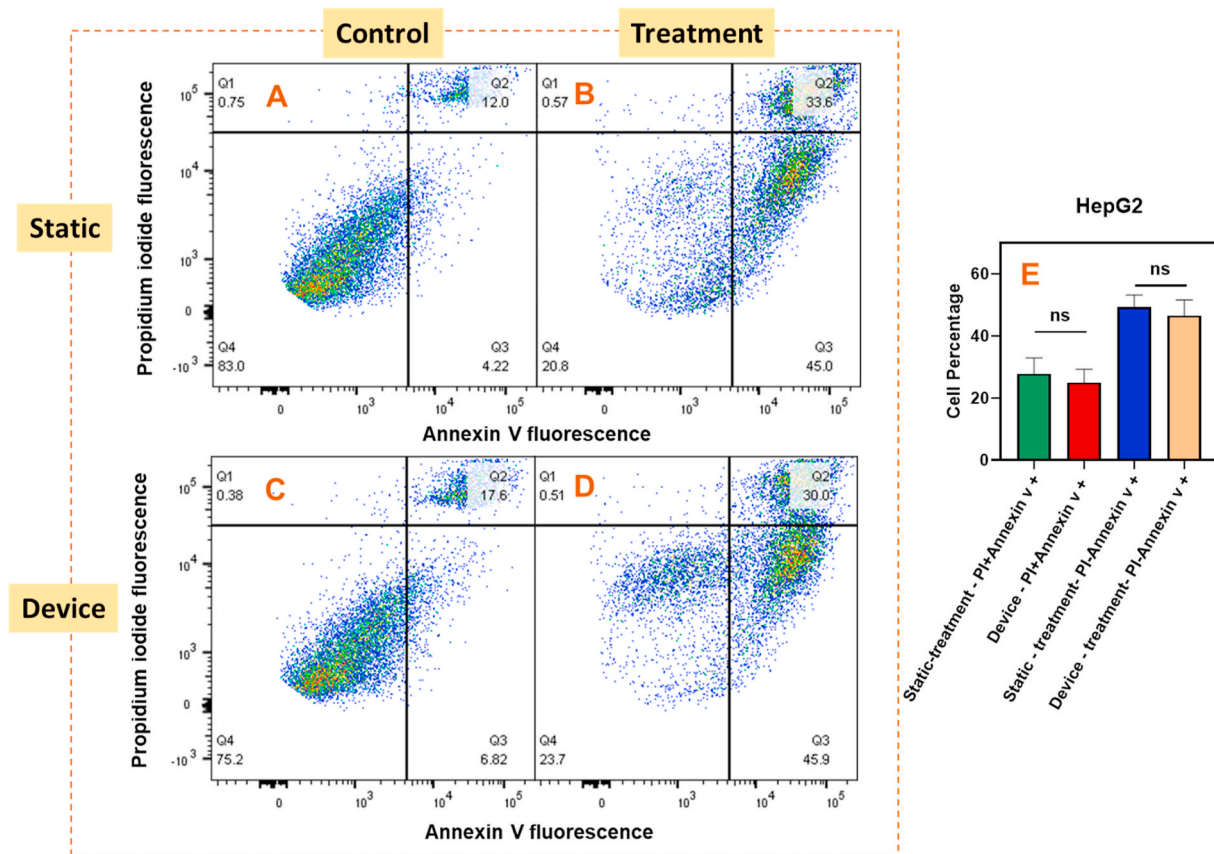


Fig. 9. Representative flow cytometry analysis of Annexin V/PI staining in HepG2 cells in two experimental setups. Conventional static 3D culture (top) and culture in the device (bottom). (A) and (C) are the control samples with no drug introduced into the system for the 3D static and device cell culture, respectively. For these control samples, only the corresponding amount of DMSO that was used for drug dissolution in treatment groups was added to the culture medium. The high population of Annexin V⁻ PI⁻ in these two groups is an indicator of the high and the comparable number of healthy HepG2 cells in these two platforms. (B) and (D) are the treatment groups (with added DOX into the culture medium) for static 3D culture and the device, respectively. Similar populations of Annexin V⁺ PI⁻ and Annexin V⁺ PI⁺ in device compared to the static culture is an indicator of the same damage patterns in this cell line. (E) Quantitative analysis of flow cytometry. Results are expressed as the percentage of the total number of the cells counted. Values are mean \pm SD. No significant difference ($0.05 < P$) was detected between the static culture and the culture within the device for the Annexin V⁺ PI⁻ and Annexin V⁺ PI⁺ populations. Error bars indicate the standard error of the means, ns = non-significant, and $n = 3$.

and its advantages over the conventional systems.

3.4. DOX metabolism

One of the proposed mechanisms for the cardiotoxic effect of DOX involves the formation of toxic metabolites, specifically DOXOL, (Hanna et al., 2014; Kamei et al., 2017) therefore, we investigated the ability of HepG2 cells to produce this metabolite *in vitro*. The HepG2 cells were treated with 1 μ M DOX, and the supernatant was harvested and analyzed using LC-MS for parent drug DOX and its metabolite DOXOL detection. The results (Fig. 8A) indicate that more than 70 % of initial DOX was metabolized by the liver cells after 72 h. Moreover, the results showed the production of DOXOL over time (Fig. 8B), which indicates that the liver cells can convert DOX to the cardiotoxic metabolite DOXOL *in vitro*. The rate and routes for the metabolism of DOX and four other anthracycline drugs have been investigated previously by Guillouzo et al. (Le Bot et al., 1988) using both rat and human adult hepatocytes. They could similarly demonstrate that both rat and human adult hepatocytes could metabolize the anthracycline drugs *in vitro*; however, the higher metabolic activity of human hepatocytes compared to rat emphasizes the differences between the species and the importance of developing a human *in vitro* model to fully capture the potential of these drugs in terms of both efficacy and adverse effects.

3.5. Drug testing in device

In the next step, we performed the drug testing on cells in the device to evaluate the toxicity of DOX and its metabolites on the liver and heart cells. As a control, a conventional 3D static culture was performed in 96 well plates. While the dynamic device is believed to recreate the interactions that generally exist between the organs (through media circulation within the device), no interactions can be observed in static controls. After drug treatments, cells were harvested, recovered from the gel, and were stained using the Alexa Fluor 488 annexin V/Dead Cell Apoptosis Kit. Phosphatidylserine (PS) within healthy cells is located in the inner surface of the cell membrane; however, in damaged apoptotic cells, PS is flipped from the inner to the outer leaflet of the plasma membrane (Van Engeland et al., 1998). Annexin V labeled with Alexa Fluor 488, can identify apoptotic cells by binding to PS exposed on the outer leaflet of the plasma membrane (Koopman et al., 1994).

Moreover, PI is a nucleic acid binding dye that can only penetrate the cells that are dead, not the live and apoptotic cells. Therefore, after staining using this kit, apoptotic cells are Annexin V⁺ PI⁻, and cell death is demonstrated in V⁺ PI⁺ populations. Fig. 9 shows that DOX had anticancer activity on HepG2 cells as a large population of apoptotic cells (V⁺ PI⁻) and dead cells (V⁺ PI⁺) are observed compared to the control. Based on the flow results, we could not detect any significant differences between the two experimental setups (3D and device) in terms of cell damage meaning the metabolite might not affect the cancer

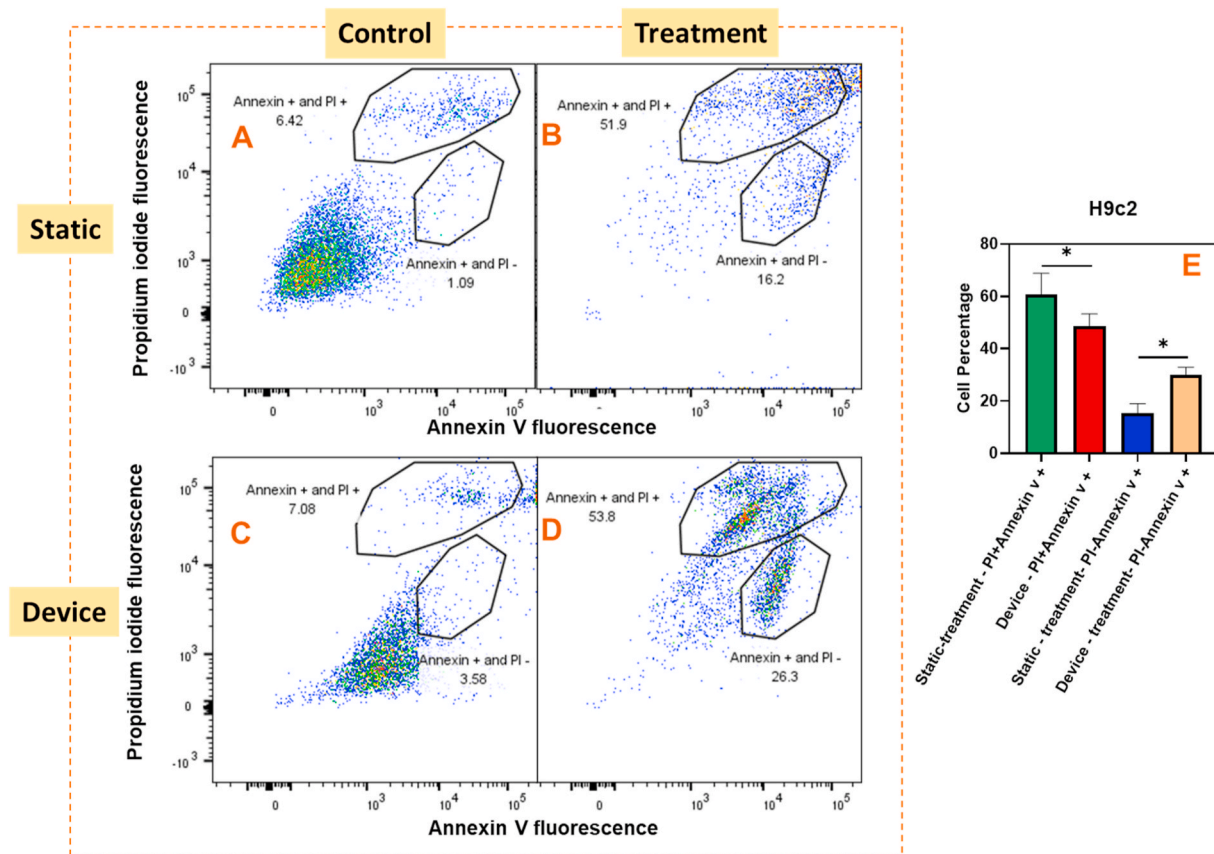


Fig. 10. Representative flow cytometry analysis of Annexin V/PI staining in H9c2 cells in two experimental setups. Conventional static 3D culture (top) and culture in the rocked device (bottom). (A) and (C) are the control samples with no drug introduced into the system for the 3D static and device cell culture, respectively. For these control samples, only the corresponding amount of DMSO that was used for drug dissolution in treatment groups was added to the culture medium. The high population of Annexin V⁻ PI⁻ in these two groups is an indicator of the high and a comparable number of healthy H9c2 cells in these two platforms. (B) and (D) are the treatment groups (with added DOX into the culture medium) for static 3D culture and the device, respectively. Higher Annexin V⁺ PI⁻ population in the device compared to the static culture is an indicator of the greater extent of damage in these cells, which can be due to the produced cardiotoxic DOXOL in the device by the metabolizing component (liver cells). (E) Quantitative analysis of flow cytometry. Results are expressed as the percentage of the total number of the cells counted. Values are mean \pm SD. There is a significant difference (P -value < 0.05) between the static culture and the culture within the device for the Annexin V⁺ PI⁻ and Annexin V⁺ PI⁺ populations. Error bars indicate the standard error of the means. Asterisks mark significance levels of $p < 0.05$ (*), and $n = 3$.

cells. However, in the case of H9c2 heart cells (Fig. 10), there was a significant difference between the apoptotic and dead cell populations in two setups. The results indicate an increase in the number of apoptotic cells (V⁺PI⁻) within the device compared to static culture. Different cell damage pattern between the device and the static culture is attributed to the exposure of heart cells to not only the parent drug but also to the metabolite being released from the HepG2 cells which reached the heart cells through the media circulation. High cardiotoxicity of DOXOL was previously observed on human cardiomyocytes in a similar microfluidic platform (Kamei et al., 2017).

4. Conclusions

One advantage of organ-on-a-chip devices is the possibility of toxicity evaluation of both parent drug and its metabolites. Here we described a heart/liver-on-a-chip device that could accommodate both HepG2 liver cells and H9c2 cardiomyocytes, which could successfully maintain both cell lines with more than 90% viability up to 5 days. Our device is pumpless, which is easy to operate based on gravity-induced flow and realistic shear stress. The fluid dynamics of the system was characterized, and the functionality of the cells in terms of urea production was evaluated. Moreover, the ability of 3D HepG2 culture to metabolize DOX *in vitro* and producing its primary metabolite (DOXOL) was investigated. Drug testing within the device demonstrated more significant damage to heart cells compared to the static culture, which is

an indicator of the exposure of the cells to both parent drug and its cardiotoxic metabolite that cannot be reproduced in conventional cell cultures. This device can be implemented as a starting point to move toward a more complex human-on-a-chip device.

Declaration of competing interest

The authors declare that they have no known competing financial interests or personal relationships that could have appeared to influence the work reported in this paper.

Acknowledgments

Financial support provided by the Welch Foundation (AT1740) is gratefully acknowledged. The generous endowed chair support from the Eugene McDermott Foundation is also acknowledged. This project was partially funded by the University of Texas at Dallas Office of Research through the Core Facility Voucher Program.

Appendix A. Supplementary data

Supplementary data to this article can be found online at <https://doi.org/10.1016/j.ooc.2021.100008>.

References

- Albini, A., Pennesi, G., Donatelli, F., Cammarota, R., De Flora, S., Noonan, D.M., 2010. Cardiotoxicity of anticancer drugs: the need for cardio-oncology and cardio-oncological prevention. *J. Natl. Cancer Inst.* 102, 14–25. <https://doi.org/10.1093/jnci/djp440>.
- Bhise, N.S., Ribas, J., Manoharan, V., 2014. Organ-on-a-chip platforms for studying drug delivery systems. *J. Contr. Release* 190, 82–93. <https://doi.org/10.1016/j.jconrel.2014.05.004>.
- Bolteyn, J., Rogiers, V., Vanhaecke, T., 2015. Functionality testing of primary hepatocytes in culture by measuring urea synthesis. *Methods Mol. Biol.* 317–321. https://doi.org/10.1007/978-1-4939-2074-7_24.
- Bottini, A.A., Hartung, T., 2009. Food for thought... on the economics of animal testing. *ALTEX*. <https://doi.org/10.14573/altex.2009.1.3>.
- Carvalho, C., Santos, R., Cardoso, S., 2009. Doxorubicin: the good, the bad and the ugly effect. *Curr. Med. Chem.* 16, 3267–3285. <https://doi.org/10.2174/092986709788803312>.
- Chegaev, K., Riganti, C., Rolando, B., 2013. Doxorubicin-antioxidant co-drugs. *Bioorg. Med. Chem. Lett* 23, 5307–5310. <https://doi.org/10.1016/j.bmcl.2013.07.070>.
- Choi, E.H., Chang, H., Cho, J.Y., Chun, H.S., 2007. Cytoprotective effect of anthocyanins against doxorubicin-induced toxicity in H9c2 cardiomyocytes in relation to their antioxidant activities. *Food Chem. Toxicol.* 45, 1873–1881. <https://doi.org/10.1016/j.fct.2007.04.003>.
- Gerlowski, L.E., Jain, R.K., 1983. Physiologically based pharmacokinetic modeling: principles and applications. *J. Pharmaceut. Sci.* 72, 1103–1127. <https://doi.org/10.1002/jps.2600721003>.
- Ghanem, A., Shuler, M.L., 2000. Combining cell culture analogue reactor designs and PBPK models to probe mechanisms of naphthalene toxicity. *Biotechnol. Prog.* 16, 334–345. <https://doi.org/10.1021/bp9901522>.
- Giridharan, G.A., Nguyen, M.D., Estrada, R., 2010. Microfluidic cardiac cell culture model (μ CCCM). *Anal. Chem.* 82, 7581–7587. <https://doi.org/10.1021/ac1012893>.
- Guan, A., Wang, Y., Guan, A., Wang, Y., 2017. Medical devices on chips. *Nat Biomed Eng* 1 (45). <https://doi.org/10.1038/s41551-017-0045>.
- Hanna, A.D., Lam, A., Tham, S., Dulhunty, A.F., Beard, N.A., 2014. Adverse effects of doxorubicin and its metabolic product on cardiac RyR2 and SERCA2A. *Mol. Pharmacol.* 86, 438–449. <https://doi.org/10.1124/mol.114.093849>.
- Hescheler, J., Meyer, R., Plant, S., Krautwurst, D., Rosenthal, W., Schultz, G., 2017. Morphological, biochemical, and electrophysiological characterization of a clonal cell (H9c2) line from rat heart. *Circ. Res.* 69, 1476–1486. <https://doi.org/10.1161/01.RES.69.6.1476>.
- Hsiao, Y.-F., Pan, H.-J., Tung, Y.-C., Chen, C.-C., Lee, C.-H., 2015. Effects of hydraulic pressure on cardiomyoblasts in a microfluidic device. *Biomicrofluidics* 9, 24111. <https://doi.org/10.1063/1.4917080>.
- Kamei, K.I., Kato, Y., Hirai, Y., 2017. Integrated heart/cancer on a chip to reproduce the side effects of anti-cancer drugs: in vitro. *RSC Adv.* 7, 36777–36786. <https://doi.org/10.1039/c7ra07716e>.
- Kim, L., Toh, Y.C., Voldman, J., Yu, H., 2007. A practical guide to microfluidic perfusion culture of adherent mammalian cells. *Lab Chip* 7, 681–694. <https://doi.org/10.1039/b704602b>.
- Kobuszewska, A., Tomecka, E., Zukowski, K., 2017. Heart-on-a-chip: an investigation of the influence of static and perfusion conditions on cardiac (H9C2) cell proliferation, morphology, and alignment. *SLAS Technol* 22, 536–546. <https://doi.org/10.1177/2472630317705610>.
- Koopman, G., Reutelingsperger, C.P.M., Kuijten, G.A.M., Keehnen, R.M.J., Pals, S.T., Van Oers, M.H.J., 1994. Annexin V for flow cytometric detection of phosphatidylserine expression on B cells undergoing apoptosis. *Blood* 84, 1415–1420. <https://doi.org/10.1182/blood.v84.5.1415.1415>.
- Le Bot, M.A., Bégué, J.M., Kernaléguen, D., 1988. Different cytotoxicity and metabolism of doxorubicin, daunorubicin, epirubicin, esorubicin and idarubicin in cultured human and rat hepatocytes. *Biochem. Pharmacol.* 37, 3877–3887. [https://doi.org/10.1016/0006-2952\(88\)90069-X](https://doi.org/10.1016/0006-2952(88)90069-X).
- Lee, S.H., Sung, J.H., 2018. Organ-on-a-Chip technology for reproducing multiorgan physiology. *Adv Healthc Mater* 7, 1–17. <https://doi.org/10.1002/adhm.201700419>.
- Lee, H., Kim, D.S., Ha, S.K., Choi, I., Lee, J.M., Sung, J.H., 2017. A pumpless multi-organ-on-a-chip (MOC) combined with a pharmacokinetic–pharmacodynamic (PK–PD) model. *Biotechnol. Bioeng.* 114, 432–443. <https://doi.org/10.1002/bit.26087>.
- Mager, D.E., Wyska, E., Jusko, W.J., 2003. Diversity of mechanism-based pharmacodynamic models. *Drug Metab. Dispos.* 31, 510–518. <https://doi.org/10.1124/dmd.31.5.510>.
- Miller, P.G., Shuler, M.L., 2016. Design and demonstration of a pumpless 14 compartment microphysiological system. *Biotechnol. Bioeng.* 113, 2213–2227. <https://doi.org/10.1002/bit.25989>.
- Misun, P.M., Rothe, J., Schmid, Y.R.F., Hierlemann, A., Frey, O., 2016. Multi-analyte biosensor interface for real-time monitoring of 3D microtissue spheroids in hanging-drop networks. *Microsystems Nanoeng* 2, 16022. <https://doi.org/10.1038/micronano.2016.22>.
- Oleaga, C., Bernabini, C., Smith, A.S., Srinivasan, B., Jackson, M., McLamb, W., Platt, V., Bridges, R., Cai, Y., Santhanam, N., 2016. Multi-Organ toxicity demonstration in a functional human in vitro system composed of four organs. *Sci. Rep.* 6, 20030. <https://doi.org/10.1038/srep20030>.
- Oleaga, C., Riu, A., Rothemund, S., 2018. Investigation of the effect of hepatic metabolism on off-target cardiotoxicity in a multi-organ human-on-a-chip system. *Biomaterials* 182, 176–190. <https://doi.org/10.1016/j.biomaterials.2018.07.062>.
- Peck, C.C., Barr, W.H., Benet, L.Z., 1992. Opportunities for integration of pharmacokinetics, pharmacodynamics, and toxicokinetics in rational drug development. *Clin. Pharmacol. Ther.* 51, 465–473. <https://doi.org/10.1038/clpt.1992.47>.
- Pistolato, F., Ohayon, E.L., Lam, A., 2016. Alzheimer disease research in the 21st century: past and current failures, new perspectives and funding priorities. *Oncotarget* 7, 38999–39016. <https://doi.org/10.18632/oncotarget.9175>.
- Polini, A., Prodanov, L., Bhise, N.S., Manoharan, V., Dokmeci, M.R., Khademhosseini, A., 2014. Organs-on-a-chip: a new tool for drug discovery 10, 1–18. <https://doi.org/10.1517/17460441.2014.886562>.
- Price, P.S., Conolly, R.B., Chaisson, C.F., 2003. Modeling interindividual variation in physiological factors used in PBPK models of humans. *Crit. Rev. Toxicol.* 33, 469–503. <https://doi.org/10.1080/10408440390242324>.
- Sin, A., Chin, K.C., Jamil, M.F., Kostov, Y., Rao, G., Shuler, M.L., 2004. The design and fabrication of three-chamber microscale cell culture analog devices with integrated dissolved oxygen sensors. *Biotechnol. Prog.* 20, 338–345. <https://doi.org/10.1021/bp034077d>.
- Soltantabar, P., Calubaquib, E.L., Mostafavi, E., Biewer, M.C., Stefan, M.C., 2020. Enhancement of loading efficiency by co-loading of doxorubicin and quercetin in thermoresponsive polymeric micelles. *Biomacromolecules* 21, 1427–1436. <https://doi.org/10.1021/acs.biomac.9b01742>.
- Sung, J.H., Shuler, M.L., 2000. A micro cell culture analog (CCA) with 3-D hydrogel culture of multiple cell lines to assess metabolism-dependent cytotoxicity of anticancer drugs. *Lab Chip* 9, 1385–1394. <https://doi.org/10.1039/b901377f>.
- Sung, J.H., Kam, C., Shuler, M.L., 2010. A microfluidic device for a pharmacokinetic–pharmacodynamic (PK–PD) model on a chip. *Lab Chip* 10, 446–455. <https://doi.org/10.1039/b917763a>.
- Sung, J.H., Wang, Y., Shuler, M.L., 2019. Strategies for using mathematical modeling approaches to design and interpret multi-organ microphysiological systems (MPS). *APL Bioeng* 3. <https://doi.org/10.1063/1.5097675>, 021501.
- Tacar, O., Sriamornsak, P., Dass, C.R., 2013. Doxorubicin: an update on anticancer molecular action, toxicity and novel drug delivery systems. *J. Pharm. Pharmacol.* 65, 157–170. <https://doi.org/10.1111/j.2042-7158.2012.01567.x>.
- Tatosian, D.A., Shuler, M.L., 2009. A novel system for evaluation of drug mixtures for potential efficacy in treating multidrug resistant cancers. *Biotechnol. Bioeng.* 103, 187–198. <https://doi.org/10.1002/bit.22219>.
- Van Engeland, M., Nieland, L.J.W., Ramaekers, F.C.S., Schutte, B., Reutelingsperger, C.P.M., 1998. Annexin V-affinity assay: a review on an apoptosis detection system based on phosphatidylserine exposure. *Cytometry* 31, 1–9. [https://doi.org/10.1002/\(SICI\)1097-0320\(19980101\)31:1<1::AID-CYTO1>3.0.CO;2-R](https://doi.org/10.1002/(SICI)1097-0320(19980101)31:1<1::AID-CYTO1>3.0.CO;2-R).
- Von Aulock, S., 2019. Is there an end in sight for animal testing? Can organ-on-a-chip replace animal use in safety testing with advanced human-focused approaches? *ALTEX* 36, 142–144. <https://doi.org/10.14573/altex.1812121>.
- Wang, Y., Lee, D., Zhang, L., 2012. Systematic prevention of bubble formation and accumulation for long-term culture of pancreatic islet cells in microfluidic device. *Biomed. Microdevices* 14, 419–426. <https://doi.org/10.1007/s10544-011-9618-3>.
- Xue, J.-X., Zhang, X.-Q., Bian, W.-H., Yao, C., 2018. Alleviation of doxorubicin-induced cardiotoxicity by Hong Huang decoction may involve a reduction in myocardial oxidative stress and activation of Akt/FoxO3a pathways. *Int. J. Clin. Exp. Med.* 11, 10574–10584.